Available online at www.sciencedirect.com
SCIENCE DIRECT®
Journal of Magnetic Resonance 163 (2003) 347–352
JMR Journal of Magnetic Resonance
www.elsevier.com/locate/jmr

Communication

Multi-scale NMR characterisation of mesostructured materials using $^{1}H \rightarrow {}^{13}C$ through-bond polarisation transfer, fast MAS, and ^{1}H spin diffusion

Bruno Alonso* and Dominique Massiot

CRMHT—CNRS, 1D avenue de la Recherche Scientifique, 45071 Orléans cedex 2, France

Received 20 December 2002; revised 14 February 2003

Abstract

A NMR method for the characterisation of materials at different length scales, robust and simple to implement, is presented. It combines selection of ^{1}H–^{13}C pairs by a through-bond polarisation transfer (INEPT here) and exploration of larger distances by the introduction of ^{1}H spin diffusion. This characterisation method is well adapted to the highest MAS rates and takes benefits of it. The effect of ^{1}H dephasing on the efficiency of the $^{1}H \rightarrow {}^{13}C$ through-bond polarisation transfer is determined. This allows consecutively the quantification of signals. Mesostructured spherical silica-based particles containing CTA^{+} cations were studied by this multi-scale characterisation method. Contrasted spin diffusion curves were found and qualitatively explained by differences in terms of mobility and spatial distributions.

Keywords: Solid state NMR; Scalar coupling; Spin diffusion; Hybrid materials; Mesoporous materials

Solid state NMR offers nowadays increasing opportunities for the characterisation of proton bearing materials at different length scales (0.1–100 nm) by combining ^{1}H high resolution and spin diffusion. Many advances are continuously made on the spectral resolution of strongly coupled nuclei like ^{1}H thanks to methodological (homonuclear decoupling [1–8]) and technological developments (high magic angle spinning (MAS) rates, associated with high magnetic fields [9]). Meanwhile, the well known cross-polarisation (CP) transfer [10] has become more precise, and thus more informative, as recently shown by with the implementation of Lee–Goldburg homonuclear decoupling [11] during contact time (CPLG). Effectively, CPLG succeeds in quenching the ^{1}H spin diffusion mechanism which usually decreases the selectivity of CP [12,13]. Under such conditions, ^{1}H–X pairs are still selected through space but at the bond scale. Alternatives to CP experiments consist in transferring the polarisation using scalar couplings *J*-based pulse sequences) instead of dipolar couplings; they allow direct through-bond selection of the ^{1}H–X pairs. Such sequences have been developed for the study of diluted molecules long time ago and are widely used in liquid state NMR [14]. In favourable cases (ca. $T_2 \geqslant J^{-1}$, vide infra), these sequences can be directly applied for the characterisation of inorganic [15] or hybrid organic–inorganic materials [16]. *J*-based polarisation transfers have even been shown to be more efficient than CP for the study of biological membranes or soft matter in general [17]. In other cases, *J*-based pulse sequences have been specifically adapted to solid state NMR by introducing ^{1}H homonuclear decoupling schemes and often a first CP step for the creation of X magnetisation [18,19]. Once the precise selection of ^{1}H–X pairs is achieved, the ^{1}H spin diffusion mechanism may be introduced separately in order to explore larger distances (up to 100 nm) [20], keeping with a through-bond encoding. The three complementary aspects: resolution, selection, and spin diffusion can thus be combined in a multi-scale NMR characterisation strategy, as already initiated with standard CP [20,21], or using CPLG [22–24].

* Corresponding author. Fax: +33-238-25-76-82.
E-mail address: alonso@cnrs-orleans.fr (B. Alonso).

1090-7807/$ - see front matter © 2003 Elsevier Science (USA). All rights reserved.
doi:10.1016/S1090-7807(03)00061-2

Our objective in this contribution was to develop a simple and robust multi-scale characterisation method combining a precise selection of ^{1}H–X bonds and ^{1}H spin diffusion, allowing the use of fast MAS and its benefits, to study mesostructured materials. These materials can be obtained from self-assembly of surfactants and mineral oligomers [25]. Their properties in terms of porosity (organised and regular pores with adjustable diameters above 2 nm), functionality (catalytic sites, hydrophobic groups, complexing agents, and many other specific functions can be incorporated), and morphology (films, fibres, or particles) render these materials very interesting. One promising development is the production of mesoporous spherical particles through evaporation induced self-assembly [26] which now allows control of the sphericity and size dispersion [27]. This family of mesostructured materials is commonly characterised by a wide panel of techniques (XRD, SEM, and TEM) that gives a particular insight to different length scales. However, one of the major difficulties is the spatial localisation of chemical groups (like a specific function) inside the mesostructure, and, in particular, with respect to an interface (organic–inorganic, oxide surface, etc.). The combined use of a precise ^{1}H–X pairs selection and of ^{1}H spin diffusion would be of great help for that purpose. We applied it to the uncalcined silica-based particles presented in Fig. 1 that are spherical in the micrometer range and mesostructured in the nanometre range, and still contain cetyltrimethylammonium (CTA^+) cations. Clearly, this multi-scale characterisation method may also be applied to a wide range of biological and organic compounds, as well as polymeric and organometallic materials.

In organic moieties, the usually largest heteronuclear J scalar couplings are $^1J_{CH}$ with values around 140 Hz ($^2J_{CH}$ and $^3J_{CH}$ are much smaller). This implies pumping delays between pulses in the millisecond range which, in rigid solids, is often far above the apparent transverse relaxation time of protons T_2^H (or more correctly the effective dephasing time of protons [28,29]) that is dominated by strong homonuclear dipolar couplings. In soft materials, intrinsic mobility diminishes homonuclear dipolar couplings and lengthens T_2^H allowing at the same time the acquisition of resolved ^{1}H MAS NMR spectra [30] and application of INEPT type pulse sequences in a simple and robust manner. We used 1D simple and refocused INEPT pulse sequences [31,32] and a modified version of the 2D correlation related sequence proposed by Bax and Morris [33]. This modified sequence is presented in Fig. 2. It contains an INEPT module for the through-bond polarisation transfer, and a mixing time τ_m for ^{1}H spin diffusion, which could be improved if necessary using an RFDR recoupling scheme [34].

1D $\{^1H\}^{13}C$ INEPT spectra (Fig. 3b) can be recorded on our samples even at moderate MAS rates ν_{MAS} (10–15 kHz), but with an improved efficiency at higher rates (20–35 kHz). Apparent ^{1}H transverse relaxation times T_2^H measured from spin-echo decays and INEPT transfer efficiency improve with increasing ν_{MAS}. This directly translates in the INEPT build up curves as a function of the Δ_1 and Δ_2 delays, corresponding to pumping and refocusing. Understanding these curves can allow measurement of the different scalar couplings, discussion of the key relaxation times, and provide quantitation of the different species. For a refocused INEPT experiment, considering a single coupling constant J_{XH}, and neglecting relaxation in a first approach, signal intensities are proportional to the product [32,35]

$$F_1(\Delta_1, \Delta_2) = n \cdot (\gamma_H/\gamma_X) \cdot G_1(\Delta_1) \cdot G_2(\Delta_2), \quad (1)$$

where n is the bond multiplicity (e.g., XH_2 and XH_3) and where

$$G_1(\Delta_1) = \sin(2\pi \cdot J_{XH} \cdot \Delta_1), \quad (2)$$

$$G_2(\Delta_2) = \sin(2\pi \cdot J_{XH} \cdot \Delta_2) \cdot \cos^{(n-1)}(2\pi \cdot J_{XH} \cdot \Delta_2). \quad (3)$$

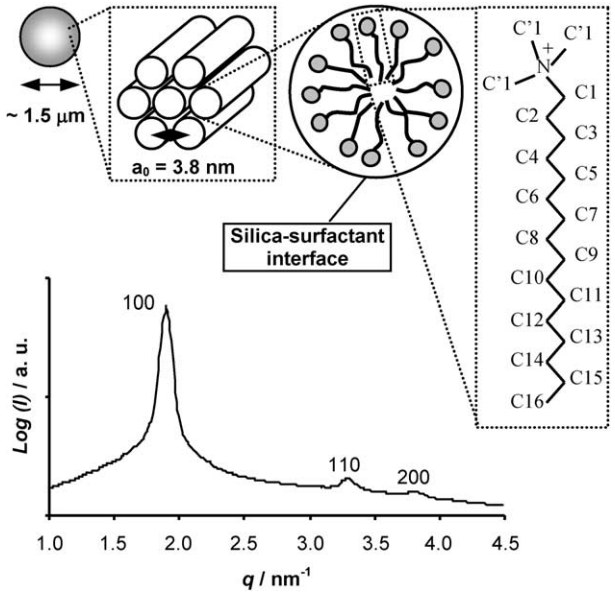

Fig. 1. Mesostructured particles were obtained by spray drying a sol aged 24 h and containing the silicon precursor (TEOS), the surfactant (CTAB), aqueous HCl (10^{-1} M), and the solvent (^{i}PrOH) in 1–0.12–5–40 molar proportions. They were dried 24 h at 110 °C and analysed by X-ray diffraction. The resulting diagram is presented above ($q = 2\pi \cdot d^{-1}$) and is assigned to a *p6mm* plane group characteristic of an hexagonal array of channels with $d_{100} = 3.3$ nm, and thus a distance between channels of 3.8 nm. The resolution of the main peak and the presence of various Bragg diffraction peaks are consistent with an extended organisation at the nanometer scale. Particles are spherical with a mean diameter of 1.5 µm as seen by scanning electronic microscopy (SEM). After calcination (500 °C during 3 h), their specific surface is in the expected range (~1000 $m^2 g^{-1}$ measured by N_2 adsorption). A study focused on the synthesis of these particles is being completed. ^{1}H and ^{13}C solid state NMR spectra of uncalcined samples correspond mainly to the signals of surfactant cation $C_{16}H_{33}(CH_3)_3N^+$ schematised above. The carbon groups have been numbered from the head to the tail.

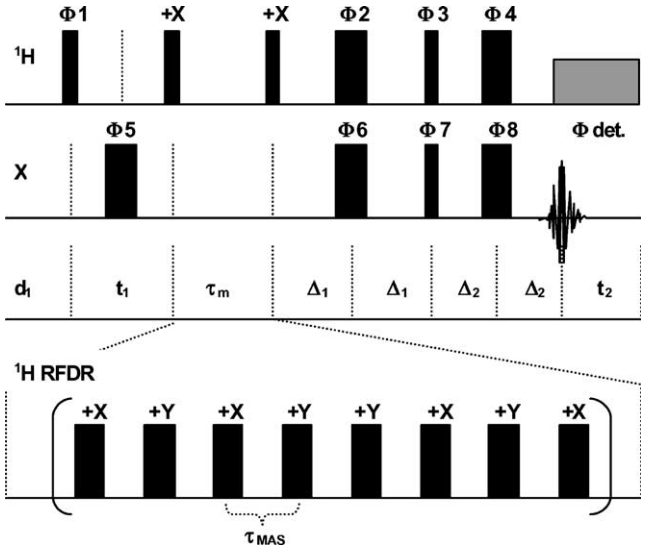

Fig. 2. Modified refocused INEPT pulse sequence for the $^1H \rightarrow {}^{13}C$ trough bond correlations. The mixing time τ_m introduced for ^1H spin diffusion may also incorporate a series of 180° ^1H recoupling pulses as in the RFDR scheme [34] in order to reintroduce ^1H dipolar couplings. Thin and large rectangles represent, respectively, 90° and 180° pulses. Phase cycling was achieved from the starting values of the INEPT sequences, adding a simple phase scheme for ^1H selection and exchange. It results in: $\phi_1 = 16\cdot\{+X\},16\cdot\{-X\};\phi_2=\phi_4=\phi_6=4\cdot\{+X,+X,-X,-X\},4\cdot\{-X,-X,+X,+X\};\phi_3=8\cdot\{+Y,-Y\},8\cdot\{-Y,+Y\};\phi_5=+X,+X,-X,-X;\phi_7=4\cdot\{+X\},4\cdot\{+Y\},4\cdot\{-X\},4\cdot\{-Y\},4\cdot\{-X\},4\cdot\{-Y\},4\cdot\{+X\},4\cdot\{+Y\};\phi_8=2\cdot\{+X,+X,-X,-X,+Y,+Y,-Y,-Y\},2\cdot\{-X,-X,+X,+X,-Y,-Y,+Y,+Y\};\phi_{det.}=2\cdot\{+X,-X\},2\cdot\{+Y,-Y\},2\cdot\{-X,+X\},2\cdot\{-Y,+Y\},2\cdot\{-X,+X\},2\cdot\{-Y,+Y\},2\cdot\{+X,-X\},2\cdot\{+Y,-Y\}$. Quadrature detection in t_1 was realised using the States method [43] and incrementing the first 90° pulse. In these conditions, and synchronising all the delays $(t_1,\tau_m,\Delta_1,\Delta_2)$ with the period of rotation τ_{MAS}, pure absorptive spectra were obtained.

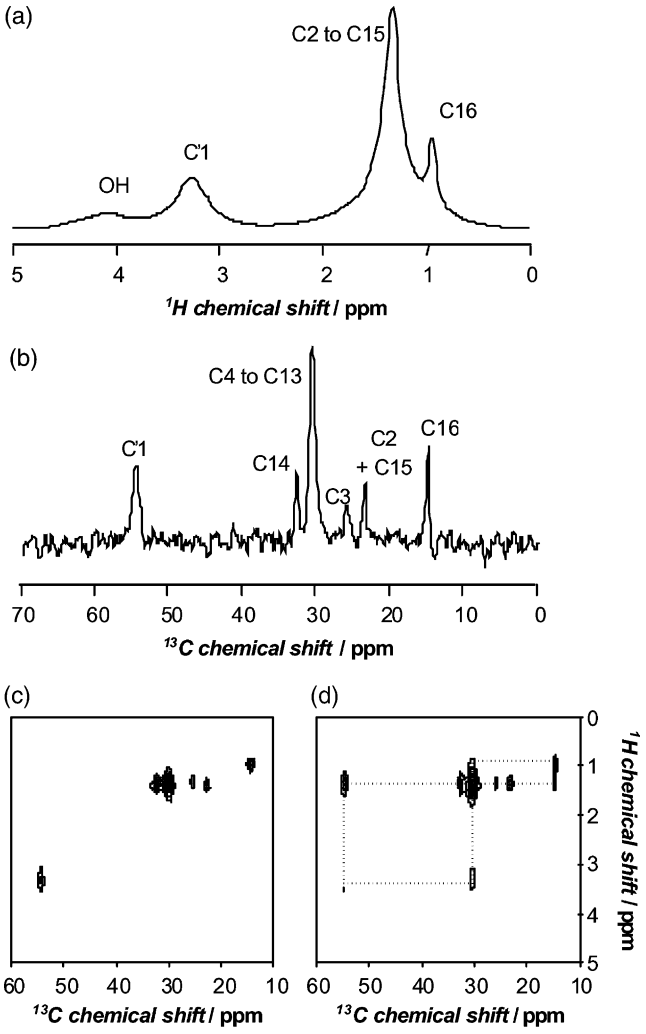

Fig. 3. (a) ^1H single pulse spectrum ($\nu_{MAS} = 25$ kHz, 4 scans); (b) $^{13}C\{^1H\}$ refocused INEPT spectrum ($\nu_{MAS} = 30$ kHz, 256 scans, $\Delta_1 = 1.0$ ms, $\Delta_2 = 0.8$ ms); (c) 2D ^{13}C–^1H INEPT spectrum ($\nu_{MAS} = 35$ kHz, $\tau_m = 0$ ms, 256 t_1 slices, 32 scans); (d) 2D ^{13}C–^1H INEPT spectrum with RFDR recoupling ($\nu_{MAS} = 35$ kHz, $\tau_m = 114$ ms, 256 t_1 slices, 64 scans). All spectra were referenced at 0 ppm relative to external TMS, and recorded on a Bruker DSX 400 ($^1H \equiv 400.13$ MHz) using 2.5 mm ZrO_2 rotors, 2 s of recycling delays and RF field strengths of 50 kHz.

Under these ideal conditions, ^{13}C signals is maximised by choosing $\Delta_1 = (4\cdot {}^1J_{CH})^{-1}$ and by adjusting Δ_2 as a function of bond multiplicities. However, in solid compounds where short T_2 does not allow to reach the maximum of efficiency of the pulse sequence, relaxation has to be considered. Figs. 4a and b present the experimental ^{13}C signal intensities obtained by varying Δ_1 and Δ_2, respectively. A very good fit of these data was obtained considering the modified function $F_2(\Delta_1,\Delta_2,T_2)$ involving a single relaxation time T_2

$$F_2(\Delta_1,\Delta_2,T_2) = F_1(\Delta_1,\Delta_2)\exp[-2(\Delta_1+\Delta_2)/T_2]. \quad (4)$$

For each site, the fitted values for J_{XH} and T_2 are in good agreement (Table 1) with measured $^1J_{CH}$, and T_2^H of the attached proton identified from 2D ^{13}C–^1H INEPT experiment (Fig. 3c). This implies that Eq. (4), for our sample, can be rewritten as

$$F_2(\Delta_1,\Delta_2,T_2) = F_2(\Delta_1,\Delta_2,T_2^H). \quad (5)$$

This empirical relationship can also be evidenced by varying ν_{MAS} (from 16.7 to 30.0 kHz) and by plotting ^{13}C signal intensities rescaled using F_1 as a function of the dephasing effect of protons (Fig. 4c). Experimental points coming from different signals were correctly correlated by an affine function.

Accurate quantification is thus reachable running series of INEPT experiments with variable delays Δ_1 or Δ_2, or at variable ν_{MAS}, and fitting the results using Eq. (5). When INEPT shows efficiency, this procedure is in fact certainly less demanding than what is required for a quantitative CP experiment [36].

Once Δ_1 and Δ_2 delays are optimised and prior to the introduction of ^1H spin diffusion ($\tau_m = 0$), the connectivity scheme of directly bound C–H pairs is established through a 2D ^{13}C–^1H INEPT spectrum (Fig. 3c). All ^{13}C and ^1H signals could be identified here except those of C1 for which T_2 values are too short. Assignments are

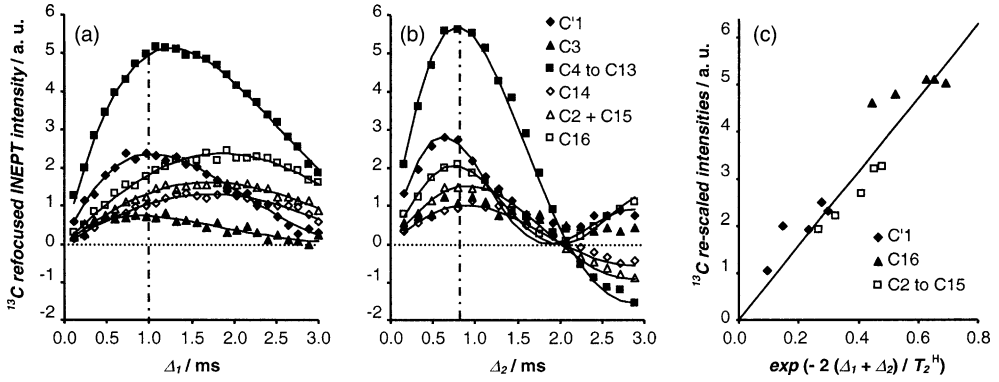

Fig. 4. (a) $^{13}C\{^1H\}$ refocused INEPT intensities plotted as a function of Δ_1 (with $\Delta_2 = 0.8$ ms) for the six sets of ^{13}C signals. For each signal, 27 experimental points ($0.12 < \Delta_1 < 3.12$ ms) were fitted by the function $n \cdot M_0 \cdot \sin(2\pi \cdot {}^1J_{XH} \cdot \Delta_1) \cdot \exp(-2 \cdot \Delta_1/T_2)$. (b) $^{13}C\{^1H\}$ refocused INEPT intensities plotted as a function of Δ_2 (with $\Delta_1 = 1.0$ ms) for the six sets of ^{13}C signals. For each signal, 30 experimental points ($0.16 < \Delta_2 < 4.64$ ms) were fitted by the function $n \cdot M_0 \cdot \sin(2\pi \cdot {}^1J_{XH} \cdot \Delta_2) \cdot \cos^{(n-1)}(2\pi \cdot {}^1J_{XH} \cdot \Delta_2) \cdot \exp(-2 \cdot \Delta_2/T_2)$. For all the spectra, 1024 scans were recorded each 2 s at $\nu_{MAS} = 25$ kHz. Vertical dashed lines correspond, respectively, to the values $\Delta_1 = 1.0$ and $\Delta_1 = 0.8$ ms selected for other 1D or 2D experiments. (c) ^{13}C signal intensities rescaled using the function $F_1(\Delta_1, \Delta_2)$ and plotted against the dephasing function $\exp(-2 \cdot (\Delta_1 + \Delta_2)/T_{2\,app.}^H)$. $^1J_{CH}$ values were taken from nonrefocused INEPT experiments (Table 1) and T_2^H were measured at five different MAS rates ($\nu_{MAS} = 16.7$, 20.0, 25.0, 28.6, and 30.0 kHz) through spin-echo experiments using mono-exponential decays. The line corresponds to the best linear fit. We found a correlation coefficient ρ above 0.93.

Table 1
^1H and ^{13}C NMR data obtained at a MAS rate of 25 kHz

Group	INEPT 2D[a]		INEPT 1D[b]	Variation Δ_1[c]		Variation Δ_2[c]		^1H echo[d]	^{13}C echo[e]
	δ^1H (ppm)	$\delta^{13}C$ (ppm)	$^1J_{CH}$ (Hz)	$^1J_{CH}$ (Hz)	T_2 (ms)	$^1J_{CH}$ (Hz)	T_2 (ms)	T_2^H (ms)	T_2^C (ms)
C′1	3.3	54.1	140 ± 10	151 ± 4	3.1 ± 0.2	134 ± 3	4.0 ± 0.4	2.44 ± 0.02	7.7 ± 0.7
C3	1.3	25.9	–	145 ± 16	2.3 ± 0.4	–	–	4.7 ± 0.1[f]	3.5 ± 0.3
C4–C13	1.4[f]	30.5	127 ± 5	117 ± 2	3.6 ± 0.1	119 ± 2	3.2 ± 0.2	4.7 ± 0.1[f]	7.6 ± 0.3
C14	1.4[f]	32.7	–	136 ± 3	23 ± 11	123 ± 2	7.0 ± 0.8	4.7 ± 0.1[f]	>20
C2 and C15	1.4[f]	23.4	122 ± 9	125 ± 4	11 ± 2	124 ± 1	11 ± 2	4.7 ± 0.1[f]	8 ± 1
C16	0.9	14.8	124 ± 1	122 ± 4	18 ± 6	125 ± 1	14 ± 1	11.8 ± 0.6	>20

[a] Chemical shift assignment done according to literature [37,44,45] and to Fig. 3.
[b] Averaged $^1J_{CH}$ scalar couplings measured for the resolved ^{13}C multiplets of seven nonrefocused INEPT spectra.
[c] $^1J_{CH}$ couplings and T_2 dephasing times obtained through the simulation of the variation of refocused INEPT ^{13}C signals as a function of Δ_1 (Fig. 4a) or Δ_2 (Fig. 4b).
[d] T_2^H apparent transverse relaxation times measured through ^1H spin-echo experiments (32 delays between 0.04 and 3.76 ms) using mono-exponential time decays.
[e] T_2^C apparent transverse relaxation times obtained through ^{13}C spin-echo experiments (without ^1H decoupling, 16 delays between 0.04 and 1.84 ms) using mono-exponential time decays.
[f] Unresolved ^1H signals.

summarised in Table 1. We notice that this 2D experiment enables to differentiate, from the main signal of the methylene groups, the ^1H signal of C3 (at ca. 1.3 ppm) that is otherwise not detectable in the 1D ^1H spectrum. With the introduction of spin diffusion, we start to explore the spatial distribution of C–H pairs. In our case, we focus on the methyl groups C′1 ($\delta_H = 3.3$ ppm, $\delta_C = 54.1$ ppm) and C16 ($\delta_H = 0.9$ ppm, $\delta_C = 14.8$ ppm) attached at to both ends of CTA^+, but complementary information could also be gained from the intermediate methylene groups. C′1 corresponds to the positively charged head group in interaction with the silica surface as it has been previously demonstrated for other mesoporous materials via ^1H–^{29}Si and ^1H–^{13}C HETCOR experiments [37]. It represents thus a signature of the silica-surfactant interface (Fig. 1). At the end of the tail, C16 is supposed to be located in the middle of CTA^+ channels. As it was observed for T_1 and $T_{1\rho}$ in other materials [38,39], we found decreasing T_2^H values from C′1 to C16 (Table 1). This trend may also account here for the variations in mobility as demonstrated for micelles and related mesophases [40,41]. In such conditions, *J*-based NMR sequences will be more efficient for the ^{13}C nuclei closest to the tail but, thanks to fast MAS, the methyl C′1 is also well detected.

However, as MAS rates are increased, the efficiency of the ^1H spin diffusion process decrease. This could be counterbalanced by the use of a recoupling procedure such as RFDR. In such conditions, we obtain much better resolved correlation peaks from ^{13}C–^1H 2D IN-

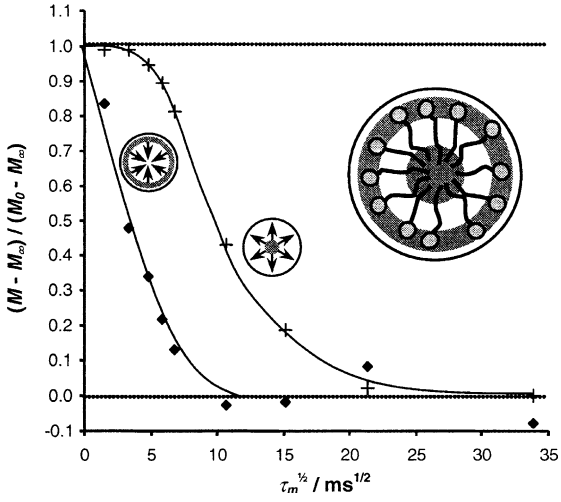

Fig. 5. Spin diffusion curves: ^{1}H–^{13}C correlation signal intensities associated to C′1 methyl groups (◆) and to C16 methyl groups (+) as a function of $\tau_m^{1/2}$. After T_1 correction [20], intensities obtained from simulation [46] of 2D ^{13}C–^{1}H INEPT spectra ran at $\nu_{MAS} = 35\,kHz$ (Fig. 3d) are normalised using the expression $(M - M_\infty)/(M_0 - M_\infty)$, where M_0 and M_∞ are, respectively, the extrapolated values at $\tau_m = 0$ and $\tau_m \to \infty$ [42]. Here, the lines are only guides for eyes.

EPT experiments recorded at increasing mixing times τ_m under fast MAS with low quantities of matter ($\nu_{MAS} = 35\,kHz$ using a 2.5 mm rotor) than under moderate MAS ($\nu_{MAS} = 10\,kHz$ using a 4 mm rotor).

Two examples of spin diffusion curves obtained at $\nu_{MAS} = 35\,kHz$ are displayed in Fig. 5. They represent the variations in intensity of correlations peaks between ^{1}H and ^{13}C signals of each C′1 and C16 groups, and thus the losses of ^{1}H magnetisation through diffusion processes from methyl groups located at the silica-surfactant interface (C′1) and from methyl groups supposedly located in the middle on CTA^+ channels (C16). The differences in mobility and the spatial distributions of the organic groups should lead to a complex spatial distribution of spin diffusion constants. Therefore, the simulation of the spin diffusion curves by solving the equation of diffusion is far from trivial as it would need a geometrical model, based on the known parameters of the mesotructure (Fig. 1), integrating these two spatial distributions. However, from the shape of the curves in Fig. 5, we can propose a picture that explains the contrasted time dependences. The variations of intensity reported as a function of $\tau_m^{1/2}$ reveal an almost constant initial rate for C′1 characteristic of a sharp interface [42]. On the contrary, the "delayed" diffusion process for C16 could signify that this group is widely distributed inside the pores. We started lattice calculations [20] based on a 2D model that seem to confirm this trend. However, simulation of the whole diffusion curves is still in progress.

In conclusion we show that this new method of multi-scale characterisation using trough bond $^{1}H \to {}^{13}C$ polarisation transfer is simple and robust. It is particularly well suited for compounds presenting some residual mobility or analysed at fast MAS, like the mesostructured materials under study. In these cases, *J*-based polarisation transfer can be used for accurate quantification of observed species in a simpler manner than with CP. In addition, X-detection instead of ^{1}H inverse detection allows to better resolve ^{1}H–X pairs from 1D spectra. As shown by looking at the effect of apparent transverse relaxation time of protons T_2^H, the range of applications will be widen at the highest MAS rates available where loss of efficiency in ^{1}H spin diffusion can be counter-balanced by implementing recoupling schemes. The spin diffusion curves resulting of series of fitted 2D ^{13}C–^{1}H correlation spectra can not be simulated easily. However, a qualitative picture based on different spatial distribution of species is proposed.

Acknowledgments

Thanks to André Douy and Emmanuel Véron for their help in the characterisation of the powders (specific surface, SEM). CNRS and European Commission—Contract HPRI 1999/00042 are acknowledged for financial support.

References

[1] R.E. Taylor, R.G. Pembleton, L.M. Ryan, B.C. Gerstein, J. Chem. Phys. 74 (1979) 4541–4545.
[2] A. Bielecki, A.C. Kolbert, M.H. Levitt, Chem. Phys. Lett. 155 (1989) 341–346.
[3] S. Hafner, H.W. Spiess, Solid State Nucl. Magn. Reson. 8 (1997) 17–24.
[4] B.-J. van Rossum, H. Förster, H.J.M. de Groot, J. Magn. Reson. 124 (1997) 516–519.
[5] E. Vinogradov, P.K. Madhu, S. Vega, Chem. Phys. Lett. 314 (1999) 443–450.
[6] D. Sakellariou, A. Lesage, P. Hodgkinson, L. Emsley, Chem. Phys. Lett. 319 (2000) 253–260.
[7] A. Lesage, L. Duma, D. Sakellariou, L. Emsley, J. Am. Chem. Soc. 123 (2001) 5747–5752.
[8] P.K. Madhu, X. Zhao, M.H. Levitt, Chem. Phys. Lett. 346 (2001) 142–148.
[9] A. Samoson, T. Tuherm, Z. Gan, Solid State Nucl. Magn. Reson. 20 (2001) 130–136.
[10] A. Pines, M.G. Gibby, J.S. Waugh, J. Chem. Phys. 59 (1973) 569–590.
[11] M. Lee, W.I. Goldburg, Phys. Rev. 140 (1965) A1261.
[12] B.-J. van Rossum, C.P. de Groot, V. Ladizhansky, S. Vega, H.J.M. de Groot, J. Am. Chem. Soc. 122 (2000) 3465–3472.
[13] V. Ladizhansky, S. Vega, J. Chem. Phys. 112 (2000) 7158–7168.
[14] R.R. Ernst, G. Bodenhausen, A. Wokaun, Principles of Nuclear Magnetic Resonance in One and Two Dimensions, Clarendon Press, Oxford, 1987.
[15] C.A. Fyfe, K.C. Wong-Moon, Y. Huang, H. Grondey, J. Am. Chem. Soc. 117 (1995) 10397–10398.
[16] B. Alonso, C. Sanchez, J. Mater. Chem. 10 (2000) 377–386.

[17] D.E. Warschawski, P.F. Devaux, J. Magn. Reson. 145 (2000) 367–372.
[18] A. Lesage, D. Sakellariou, S. Steuernagel, L. Emsley, J. Am. Chem. Soc. 120 (1998) 13194–13201.
[19] A. Lesage, L. Emsley, J. Magn. Reson. 148 (2001) 449–454.
[20] K. Schmidt-Rohr, H.W. Spiess, Multidimensional Solid-State NMR and Polymers, Academic Press, London, 1994.
[21] D. Massiot, B. Alonso, F. Fayon, F. Fredoueil, B. Bujoli, Solid State Sci. 3 (2001) 11–16.
[22] D. Huster, X. Yao, M. Hong, J. Am. Chem. Soc. 124 (2002) 874–883.
[23] B. Alonso, I. Klur, D. Massiot, Chem. Commun. (2002) 804–805.
[24] B. Alonso, F. Fayon, F. Fredoueil, B. Bujoli, D. Massiot, J. Sol–Gel Sci. Technol. 26 (2003) 95–98.
[25] C. Kresge, M. Leonowicz, W. Roth, C. Vartuli, J. Beck, Nature 359 (1992) 710–712.
[26] Y. Lu, H. Fan, A. Stump, T.L. Ward, T. Rieker, C.J. Brinker, Nature 398 (1999) 223–226.
[27] G.V. Rama Rao, G.P. Lopez, J. Bravo, H. Pham, A.K. Datye, H. Xu, T.L. Ward, Adv. Mater. 14 (2002) 1301–1304.
[28] A. Lesage, S. Steuernagel, L. Emsley, J. Am. Chem. Soc. 120 (1998) 7095–7100.
[29] S.P. Brown, M. Pérez-Torralba, D. Sanz, R.M. Claramunt, L. Emsley, Chem. Commun. (2002) 1852–1853.
[30] L. Camus, V. Goletto, J. Maquet, C. Gervais, C. Bonhomme, F. Babonneau, D. Massiot, J. Sol–Gel Sci. Technol. 26 (2003) 311–314.
[31] G.A. Morris, R. Freeman, J. Am. Chem. Soc. 101 (1979) 760–762.
[32] D.P. Burum, R.R. Ernst, J. Magn. Reson. 39 (1980) 163–168.
[33] A. Bax, G.A. Morris, J. Magn. Reson. 42 (1981) 501–505.
[34] A.E. Bennet, J.H. Ok, R.G. Griffin, S. Vega, J. Chem. Phys. 96 (1992) 8624–8627.
[35] P. Lux, F. Brunet, H. Desvaux, J. Virlet, Magn. Reson. Chem. 31 (1993) 623–631.
[36] W. Kolodziedjski, J. Klinowski, Chem. Rev. 102 (2002) 613–628.
[37] M.T. Janicke, C.C. Landry, S.C. Christiansen, D. Kumar, G.D. Stucky, B.F. Chmelka, J. Am. Chem. Soc. 120 (1998) 6940–6951.
[38] R. Simonutti, A. Comotti, S. Bracco, P. Sozzani, Chem. Mater. 13 (2001) 771–777.
[39] D. Kubies, R. Jérôme, J. Grandjean, Langmuir 18 (2002) 6159–6163.
[40] R. Bacaloglu, A. Blaskó, C.A. Bunton, G. Cerichelli, A. Shirazi, Langmuir 7 (1991) 1107–1111.
[41] N. Mahieu, P. Tekely, J.-C. Boubel, J.M. Cases, D. Canet, J. Phys. Chem. 97 (1993) 9513–9518.
[42] D.L. VanderHart, G.B. McFadden, Solid State Nucl. Magn. Reson. 7 (1996) 45–66.
[43] D.J. States, R.A. Haberkorn, D.J. Ruben, J. Magn. Reson. 48 (1982) 286–292.
[44] W. Kolodziejski, A. Corma, M.-T. Navarro, J. Pérez-Pariente, Solid State Nucl. Magn. Reson. 2 (1993) 253–259.
[45] F. Kleitz, J. Blanchard, B. Zibrowius, F. Schüth, P. Ågren, M. Linden, Langmuir 18 (2002) 4963–4971.
[46] D. Massiot, F. Fayon, M. Capron, I. King, S. Le Calvé, B. Alonso, J.-O. Durand, B. Bujoli, Z. Gan, G. Hoatson, Magn. Reson. Chem. 40 (2002) 70–76.